Tellus (2008), 60A, 216–233
Printed in Singapore. All rights reserved

TELLUS

Sensitivity Observing System Experiment (SOSE)—a new effective NWP-based tool in designing the global observing system

By GERT-JAN MARSEILLE*, AD STOFFELEN and JAN BARKMEIJER, *KNMI, Wilhelminalaan 10, 3732 GK De Bilt, The Netherlands*

(Manuscript received 15 January 2007; in final form 15 October 2007)

ABSTRACT

Lacking an established methodology to test the potential impact of prospective extensions to the global observing system (GOS) in real atmospheric cases we developed such a method, called Sensitivity Observing System Experiment (SOSE). For example, since the GOS is non uniform it is of interest to investigate the benefit of complementary observing systems filling its gaps. In a SOSE adjoint sensitivity structures are used to define a pseudo true atmospheric state for the simulation of the prospective observing system. Next, the synthetic observations are used together with real observations from the existing GOS in a state-of-the-art Numerical Weather Prediction (NWP) model to assess the potential added value of the new observing system. Unlike full observing system simulation experiments (OSSE), SOSE can be applied to real extreme events that were badly forecast operationally and only requires the simulation of the new instrument. As such SOSE is an effective tool, for example, to define observation requirements for extensions to the GOS. These observation requirements may serve as input for the design of an operational network of prospective observing systems. In a companion paper we use SOSE to simulate potential future space borne Doppler Wind Lidar (DWL) scenarios and assess their capability to sample meteorologically sensitive areas not well captured by the current GOS, in particular over the Northern Hemisphere oceans.

1. Introduction

Many resources are spent on new observation types complementing the meteorological global observing system (GOS) or its climate equivalent (GCOS). The current observing system is rather non-uniform lacking observations over the oceans, tropics and Southern Hemisphere resulting in rather non-uniform errors in NWP analyses and subsequent forecast failures. International programs such as the observing system research and predictability experiment (THORPEX), Shapiro and Thorpe (2004), show a growing interest to define an observational network that increases the accuracy of high-impact weather forecasts. This addresses fundamental questions related to observation strategies such as the relative merit of new polar orbiting satellites, giving a uniform global coverage of observations, against, for example, targeting strategies where additional observations are constrained to pre-determined meteorologically sensitive areas.

This paper presents a new and relatively cheap method to assess the added value of additional observations for NWP. The proposed method provides an easy way to test various observation strategies culminating in observation requirements for prospective observing systems for instance to sample meteorologically sensitive areas that are otherwise not measured. These sensitive areas are generally associated with atmospheric structures that tend to grow rapidly in time potentially causing forecast failures already on the short term (up to 2 d).

The potential value of new observations for weather and climate analyses depends on (i) the information content of the new observing system and its fundamental ability to complement the existing G(C)OS in describing the atmospheric circulation and mass field and (ii) the ability of the (future) data assimilation system to exploit this new information. The first requirement is a prime, the second is often problematic in existing data assimilation systems. These are often not well tuned to exploit the new data types and extended trials are needed to test the consistency of the new data with the forecast model and analysis scheme characteristics. A greater consistency of observations and the data assimilation system is generally achieved in Observing System Experiments (OSE), for example, Kelly (2004) or Observing System Simulation Experiments (OSSE), but for different reasons. The assimilation of existing observing systems is already tuned for beneficial analysis impact in OSE, whereas simulated

*Corresponding author.
e-mail: Gert-Jan.Marseille@knmi.nl
DOI: 10.1111/j.1600-0870.2007.00288.x

(future) observing systems in OSSE may not fully capture the real observation error characteristics. However, OSSE calibration should guarantee the appropriate observing system impact (e.g. Stoffelen, 2006; Masutani et al., 2004). OSSE test the analysis and forecast impact of future and thus non-existing observing systems, whereas OSE test the impact of existing observing systems. OSE thus provide real impact of real observations in a given data assimilation system. The OSE are used to further test and improve the assimilation of certain data types, and to test the relevance of the different existing components of the GOS (WMO, 2004). Gaps in the GOS, for example the lack of wind profile data over the oceans, tropics and Southern Hemisphere can be filled by new observing systems. OSE cannot test the expected impact of such observations, since no existing observing system provides these data. OSE or Observation System Replacement Experiments (OSRE) could for example be used, respectively, to test the impact of existing wind profile observations over Northern Hemisphere land or how these may be replaced by another observing system (Cress and Wergen, 2001). Although indicative, it is however a priori not clear how exactly to extrapolate these results to the case of more uniform and complete wind profile coverage over the globe. To overcome this problem OSSE may be conducted, realistically simulating the atmosphere, all existing and newly expected observing systems, and thus conditioning the appropriate sensitivity of the given data assimilation system to these different observation types (Stoffelen et al., 2006). However, not for all existing observing sytems the observation error covariance matrix is well known like in the case of satellite radiance data. Yet for a realistic impact assessment they need to be accurately simulated in an OSSE. It may be clear that OSSE require many human resources.

Other methods exist that investigate the information content of observing systems, such as analysis ensemble methods (Tan et al., 2007) that uses the spread in the ensemble as a proxy of analysis or background uncertainty based on arguments of linear error growth (Fisher, 2003). The method requires correct knowledge of observation error covariances that are generally unknown and as such some of the limitations due to unknown errors in OSSE do also exist in analysis ensemble methods. In addition, if the method is to be applied for prospective observing systems and in forecast mode, then for simulation purposes a truth at analysis time needs to be assumed, for example, the ensemble mean, which will anyway be associated with multivariate and spatially correlated error that would affect the forecast results and its spread.

Hello et al. (2000) focus on extreme weather and use adjoint sensitivity structures to correct the analysis and observations to tune the amplitude of these structures. However, their objective differs from ours and is to provide guidance to operational forecasters with a tool to investigate alternatives to the reference forecast. As such the adjoint sensitivity computation is used a priori to find meteorologically sensitive areas and corresponding sensitive structures. Their approach requires tuning of the amplitude of the sensitivity structures using existing observations in the sensitive area. A single tuning parameter is used for this purpose whose optimal value depends strongly on the data set used. Small values indicate that the sensitivity structures do not well correlate with the analysis error, thus potentially increasing the analysis error. In addition, the generated structures are not constrained to reduce the forecast error, by construction. Although useful for operational practice this approach reveals practical problems for the simulation of prospective observing systems and their use together with existing observing systems in data assimilation and was found not suitable for our purposes.

The aforementioned methods are useful in itself, but they are not directly applicable to assess the added value of prospective observing system to sample the unobserved component of the atmospheric state and to better forecast real (extreme) events. For this purpose we developed a new method named Sensitivity Observing System Experiment (SOSE). The major component of a SOSE is the definition of a synthetic true atmospheric state, hereafter named 'pseudo-truth', that is needed for the simulation of the new observing system under investigation. The pseudo-truth is defined as an adapted forecast initial state (analysis). To adapt the analysis we use adjoint sensitivity structures that are a proxy of the part of the analysis error that grows most rapidly in time and as such potentially causing large forecast failures if not observed. In Section 2, it is shown that the operational mode to compute sensitivity structures does not meet the pseudo-truth requirements. A new concept based on background sensitivities is described and it is shown that the resulting analysis adaptations have realistic spatial structures, are in agreement with observations of existing observing systems and as such constitute that part of the sensitivity structures that is not observed by the existing observation network. New observing systems may fill in to observe these structures. Analysis and forecast experiments including real observations from existing observing systems and synthetic observations from the new instrument demonstrate the capability of the new observing system to measure the structures that are not observed by the existing observing network. Section 3 describes the mathematical framework of SOSE explaining the need for a tuning procedure for a correct weighting of synthetic observations in a SOSE. A case study demonstrates the tuning procedure for future spaceborne Doppler wind lidar (DWL) measurements. Section 4 provides the summary and conclusions and recommendations for further developments of the SOSE method. A list of acronyms is provided in Table 2 at the end of the paper.

2. Definition of a synthetic pseudo-true atmosphere

An important aspect of observation impact experiments of yet non-existing observing systems is the need for an atmospheric state for the simulation of the new observing system. Since the true atmosphere is inherently unknown a synthetic atmosphere

state, in the remainder denoted 'pseudo-truth', needs to be defined. In SOSE the pseudo-truth is defined as an adapted analysis. The analysis is the result of merging observations into the NWP model in a statistically optimal way and is the best available estimate of the atmospheric state at forecast initial time. However, errors in the analysis can be quite significant in data sparse regions such as the Southern Hemisphere, Tropics and Northern Hemisphere oceans. These errors may grow rapidly in time to give large forecast failures already on the short term (first 48 h). The pseudo-truth should correct for these key errors in the incorrect analysis with the constraint that analysis departures of existing observations do not increase. As such the pseudo-truth is a better forecast initial state and in agreement with existing observations. Summarizing, the pseudo-truth is an adapted analysis that should fulfil the following three requirements, in the remainder denoted R1–R3. The pseudo-truth

(1) improves the 2-d forecast (R1), but still
(2) is compatible with existing (real) observations (R2) and
(3) has realistic spatial structures, that is, analysis adaptations should resemble real analysis errors (R3).

The pseudo-truth is subsequently used for the simulation of the future observing system under investigation and when the new observing system is capable of (partly) observing the analysis adaptations, it will contribute to improve the 2-d forecast.

A similar approach was adopted by Bergot et al. (1999) where they select two different forecast initial states for the same case, one (the control) giving a bad, the other (say, the pseudo-truth) giving a good forecast. The objective then is to correct the bad analysis with additional (targeted) observations to reduce the distance between the two forecasts. Synthetic observations are obtained from the pseudo-truth over a pre-determined meteorologically sensitive area. A limitation of this approach is that for real extreme events it is not trivial to select a forecast initial state that verifies 2 d later and fulfils the GOS compatibility constraint (R2).

An obvious choice to correct the analysis is to use adjoint sensitivity structures since they fulfil R1 by construction. In addition, sensitivity structures are a proxy for the part of the analysis error that grows most rapidly in time and as such potentially causing large forecast failures if not observed. The concept of adjoint sensitivity structures and their use in SOSE is discussed in the next section.

2.1. *The use of adjoint sensitivity structures to correct the analysis*

Adjoint sensitivity computations were performed operationally at ECMWF until medium 2005 as a diagnostic tool to trace back forecast errors to rapidly growing errors in the forecast initial state. An extensive description of adjoint sensitivity computations is found in Rabier et al. (1996), Klinker et al. (1998) and Isaksen et al. (2005). A posteriori, in case of a failing forecast, one could in principle try to modify the trajectory of the forecast in order to better forecast the analysed extreme event. This can be achieved by correcting the forecast initial state and/or adding model tendency perturbations to account for model errors (Barkmeijer et al., 2003). In our study, model errors are not considered. Only that part of the forecast error ascribed to an imperfect analysis is taken into account. A sensitivity computation then provides an adaptation of the incorrect analysis that represents the part of the analysis error that grows most rapidly in time and would have reduced the 2-d forecast error by a about a factor of two (Rabier et al., 1996). The mathematical framework of adjoint sensitivity computations is found in the Appendix. In a weak constraint approach (Trémolet, 2006) one would expect a much larger forecast error reduction due to accounting for model error. A consequence of the perfect model assumption may be that (part of) the model errors are projected onto the analysis error, potentially giving unrealistic analysis adaptations. Current understanding is that errors in the forecast initial conditions play a more important role in the initial stage of the forecast (up to 2 d) at least in the extra-tropical regions, whereas the model error becomes increasingly more important in the medium range (Bergot et al., 1999). Also it is known from studies of extreme cases in the past that single observations that were rejected by the assimilation quality control system would have improved the forecast substantially when used in the analysis, indicating that both dynamics and physics of the models are sufficient to resolve the relevant processes (Hello et al., 2000). For the 1997 and 1999 Christmas storm cases over Britain and Germany/France 84-h forecasts verified better than the short-range (36–48 h) forecasts, another indication of imperfect use of observations in data assimilation and less of model errors (Hello et al., 2000).

The computed spatial structure improving the initial analysis is called sensitivity structure. These sensitive structures are also denoted 'key analysis errors', suggesting that they explain most or at least a significant part of the analysis error as demonstrated by Klinker et al. (1998) in a case study. However a more extensive evaluation by Isaksen et al. (2005) over a 2-month period showed no correlation between analysis errors and adjoint sensitivity structures, in fact analysis errors increase on average when corrected with sensitivity structures. Other studies confirm this result, for example, Bergot et al. (1999), Hello et al. (2000) and during the Atlantic THORPEX Regional Campaign (A-Trec) in 2003, Koch et al. (2006) found no correlation between analysis departures of passively assimilated airborne DWL observations and corresponding computed key analysis errors.

This discrepancy between real analysis errors and computed 'key analysis errors' may be surprising considering the mutual objective of data assimilation and sensitivity computations to find an optimal forecast initial state. Yet, both methodologies differ principally, that is, data assimilation draws the initial state to the true atmosphere by finding an optimal balance between the forecast model and atmospheric observations, while a sensitivity computation finds an adaptation for the incorrect analysis

a posteriori with the only objective to reduce the forecast error but with no explicit constraint to available observations. Secondly, the phase and spatial structures of the sensitivity structures are closely linked to the used norms in the sensitivity computation (see Appendix). Some norm candidates were evaluated by Palmer et al. (1998) and Isaksen et al. (2005) showing that substantial different adaptations at forecast initial time evolve into about equal forecast adaptations after 2 d. More principally, one should not expect an adjoint computation, that does not take into account observations, could recover real analysis error structure and phase 2 d earlier due to the limited predictability of the atmospheric state. Finally, sensitivity structures describe only the fast growing modes of the analysis error, see Rabier et al. (1996), and therefore represent only a small fraction of the complete analysis error by construction.

However, for a realistic assessment of observation impact in NWP we argue that exact knowledge of the *real* analysis error is not a pre-requisite. The added value of observations in data assimilation is closely related to their capability to resolve the spatial structures of the analysis error. As such, for the definition of the pseudo-truth, it is sufficient that analysis adaptations are *realistic* in the sense that their spatial structures resemble those of real analysis errors.

As demonstrated by Isaksen et al. (2005), adjoint sensitivity structures are not compatible to available observations thus violating the observation requirement (R2). For this reason the observation compatibility constraint is embedded in the SOSE approach by computing key *background* errors, that is, instead of using the analysis as forecast initial state, as in operational mode, the background is used as forecast initial state to obtain the forecast error for the adjoint sensitivity computation. The resulting sensitivity structures are used to adapt the background. The adapted background is subsequently merged with the existing observations to produce the SOSE analysis. The validity of the SOSE analysis to represent the pseudo-truth is verified by checking R1–R3. This two-step procedure of a background sensitivity computation followed by an analysis is visualized in Fig. 1. The rationale behind this approach is that background sensitivity structures are corrected in data dense areas to match with existing observations while they are maintained in data sparse regions. Therefore the resulting key SOSE adaptations (SOSE analysis—control analysis) constitute that part of the sensitivity structures that is not observed by the existing observation network. New observation systems may fill in to observe these structures. We will show that the key background error variance is reduced by about 50% in the SOSE analysis step, that is, the SOSE analysis maintains about 50% of the key background adaptation and subsequent forecast error reduction capability. The realism of adjoint sensitivity structures and key SOSE adaptations for the definition of the pseudo-truth is tested in the next section in the framework of an OSSE.

2.2. *Use of OSSE to validate sensitivity structures*

The realism of adjoint sensitivity structures and their suitability for the definition of the pseudo-truth is discussed in this section within the framework of an OSSE, because it offers the unique property of knowing the true synthetic atmospheric state, through the nature run, see the first bullet below. This facilitates the verification of sensitivity structures not only at observation locations, for example, as in Isaksen et al. (2005) but also in data sparse areas were sensitivity structures are most pronounced. To make the

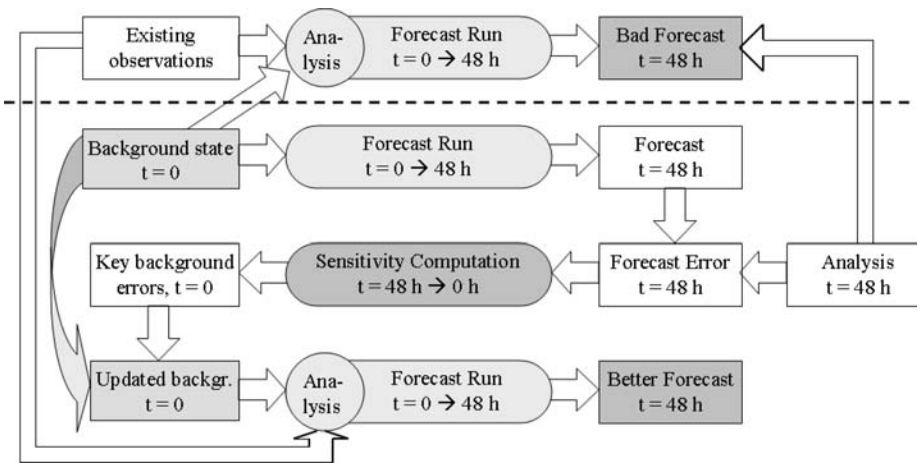

Fig. 1. SOSE analysis scheme. The top row shows a standard analysis experiment where observations are merged with the background. The resulting bad forecast is improved by the SOSE procedure in the subsequent rows below the dashed line. The second row shows a 48-h forecast initiated with the background. In the third row the forecast error (forecast minus verifying analysis) is projected back in time through a sensitivity computation to give key background errors to correct the background. The corrected background is merged with observations of existing observing systems in the analysis to provide a better forecast initial state. The SOSE analysis in the fourth row is also named pseudo-truth.

verification transparent we used the same model version for the analysis and sensitivity experiments, to avoid mixing of different model versions in the sensitivity computations potentially yielding unrealistic sensitivity structures. To that end the 1999 OSSE experiment described in Stoffelen et al. (2006) was repeated with a more recent version (cycle 26r3) of the ECMWF forecast model that was operational from October 2003 to March 2004. A similar setup as the 1999 OSSE was chosen for the analysis and forecast experiments. The main characteristics are summarized below.

(1) A nature run representing a true synthetic atmospheric state, obtained from a 30-d integration of the 1993 ECMWF operational model over the period 5 February–7 March 1993. The horizontal resolution is about 100 km with 31 levels in the vertical (T213L31).

(2) Simulated observations representing the 1993 observation coverage but excluding TOVS radiances, see Stoffelen et al. (2006).

(3) 4D-Var data assimilation (Rabier et al., 2000) using a recent model version. The assimilation period extends from 5 February 1993 to 20 February 1993, with a 6-h assimilation window.

Good agreement between analyses of both OSSE experiments was found above the data dense continents with the largest differences mainly found over the oceans, in particular over the tropics and southern hemisphere reflecting the evolution of the ECMWF model over the 1999–2004 period (not shown). We stress that SOSE is designed to apply to real events for which the truth is not known. The OSSE framework, for which the truth *is* known, is used to verify the various options to produce the SOSE pseudo-truth as discussed in the sequel.

2.2.1. Sensitivity computations for the OSSE period. The OSSE experiment extended over the period 5 February to 20 February 1993. Analyses and forecasts were produced at a 6-h time interval. They serve as input for the sensitivity computations. Sensitivity computations were conducted in two modes:

(1) Operational (or default) mode. This is the usual way of using the analysis as forecast initial state to obtain the forecast error used in the sensitivity computation, see for example, Rabier et al. (1996), Klinker et al. (1998), Isaksen et al. (2005). The resulting sensitivity structures are added to the analysis to give the adapted analysis. Analysis adaptations produced in operational mode are in the remainder denoted ANSENS.

(2) SOSE mode. Here the background, $\mathbf{x}_b$, is used as forecast initial state. The forecast error from the 48-h forecast initiated with $\mathbf{x}_b$ minus the verifying analysis is used in the sensitivity computation, see Fig. 1. The resulting sensitivity structures, $\delta\mathbf{x}_b$, are in the remainder denoted BGSENS.

ANSENS and BGSENS have been determined for the 16-d OSSE period using 12 UTC analyses and 9 UTC backgrounds as forecast initial state, respectively. The target area is the northern hemisphere extra-tropics north of 30° latitude. For both the operational and SOSE mode, total energy (TE) and **B**-matrix norm sensitivities were determined. For TE norm sensitivities, the total energy norm is used as initial time norm in the sensitivity computation, see the Appendix for further details. The spatial scales of TE norm sensitivities show large resemblance with the scales of analysis errors (Palmer et al., 1998), however the temperature and wind perturbations are geostrophically unbalanced (Caron et al., 2007). Using the background error covariance matrix, denoted **B**-matrix, as initial time norm in the sensitivity computation yields perturbations that are in geostrophical balance. The resulting spatial structures are much broader than for TE norm perturbations. This is visualized in Fig. 2. The amplitude of the temperature perturbation is larger for the TE norm while the reverse is true for the wind perturbation. Also the vertical structures in Fig. 3 are broader for the **B**-matrix norm and the maximum amplitude is found near 600 hPa for TE norm and near 300 hPa for **B**-matrix norm perturbations. Not surprisingly BGSENS and ANSENS show close correspondence (not shown).

The total energy spectra and vertical distributions of total energy in Fig. 4 confirm that TE/**B**-matrix norm sensitivities put most of the energy in temperature/wind adaptations with maximum values near 600 hPa for the TE and 450 hPa for the **B**-matrix norm. The spectrum of TE norm sensitivities in the lower left panel of Fig. 4 is rather flat meaning that all spatial scales are represented equally well in terms of TE norm. The **B**-matrix norm sensitivities in the lower right-hand panel on the other hand show a clear peak near wavenumber 12 (1500 km scale structures) and minimal energy for high wavenumbers (smaller spatial scales).

To obtain the SOSE analysis, BGSENS is added to the background to obtain the adapted background: ($\tilde{\mathbf{x}}_b = \mathbf{x}_b + \delta\mathbf{x}_b$). The adapted background is merged with observations to give the adapted (SOSE) analysis: $\mathbf{x}_a = \tilde{\mathbf{x}}_b + \mathbf{K}[\mathbf{y} - \mathbf{H}\tilde{\mathbf{x}}_b]$, with $\mathbf{K}$ the gain matrix and $\mathbf{H}$ the observation operator as explained in Section 3.1. Figs. 5 and 6 show the resulting analysis adaptation, $\delta\mathbf{x}_a$, at background time, that is, at the beginning of the 6-h assimilation window in a 4D-Var context. Here the analysis adaptation $\delta\mathbf{x}_a$ or ANSOSE for future reference is defined as ANSOSE = SOSE analysis - ANCNTL, with ANCNTL the control analysis obtained from $\mathbf{x}_a^c = \mathbf{x}_b + \mathbf{K}\,[\mathbf{y} - \mathbf{H}\mathbf{x}_b]$. Then ANSOSE equals $\delta\mathbf{x}_a = \mathbf{x}_a - \mathbf{x}_a^c = [\mathbf{I} - \mathbf{KH}]\delta\mathbf{x}_b$, whose averaged amplitude is generally about 50% smaller than $\delta\mathbf{x}_b$ due to the merging with observations. This is also clear from Figs. 2 and 5 that show that background sensitivities have been corrected by observations over the data dense continents, while they are maintained to a large extent over the data sparse oceans.

The capability of sensitivity structures to improve the 2-d forecast is visualized in Fig. 7 that shows the root mean square (RMS) forecast errors over the complete OSSE period for forecasts initiated with non-adapted (control) analyses and adapted analyses, according to ANSENS and ANSOSE, respectively. Here RMS

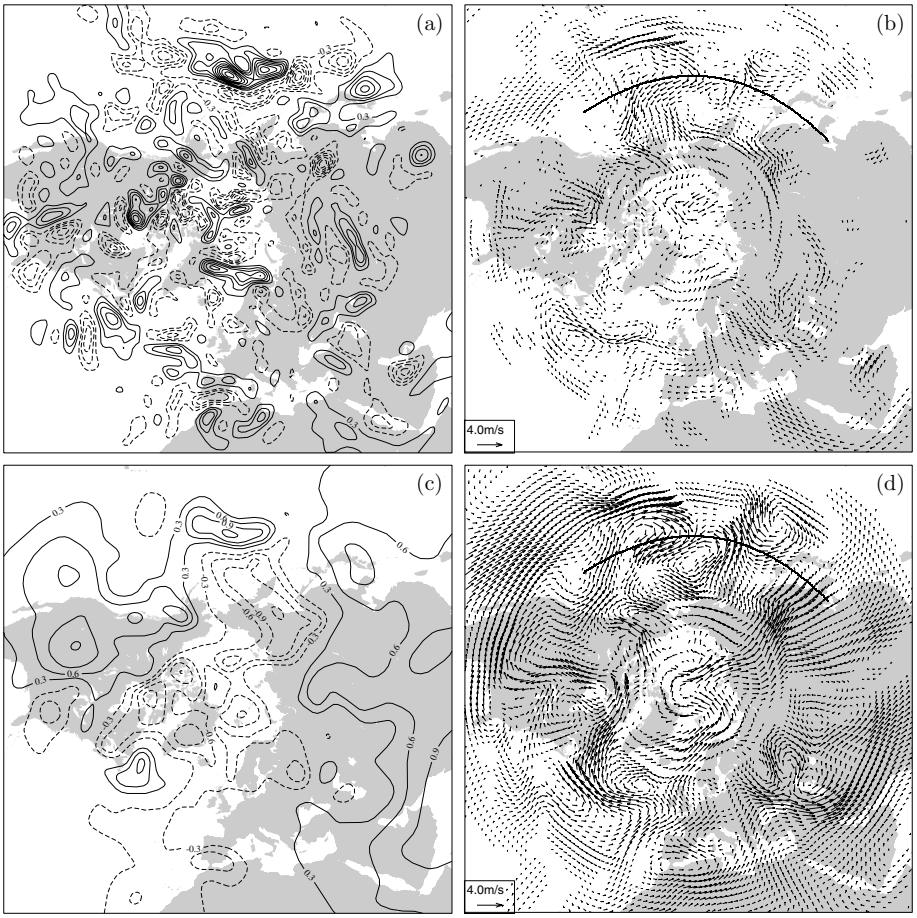

Fig. 2. OSSE 500 hPa background sensitivity perturbations, BGSENS, for 10 February 1993 9 UTC. Temperature (K) and wind (ms^{-1}) perturbations based on TE (a,b) and **B**-matrix (c,d) initial time norm sensitivity computations. The contour interval is 0.3 K. Solid/dashed contour lines are for positive/negative values. The solid thick lines over the Pacific near 40°N show the location of the vertical cross-section displayed in Fig. 3.

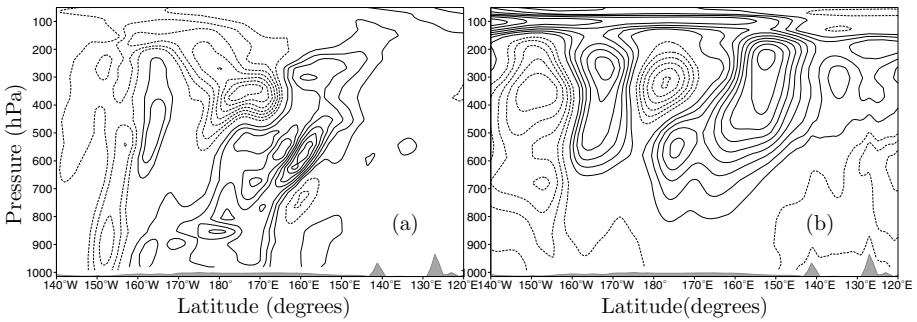

Fig. 3. Cross-section of zonal wind component sensitivity perturbations (BGSENS) over the Northern Pacific near 40°N (see Fig. 2) for 10 February 1993 9 UTC based on a (a) TE norm and (b) **B**-matrix norm sensitivity computation. The contour interval is 0.25 ms^{-1}. Solid/dashed contour lines are for positive/negative values.

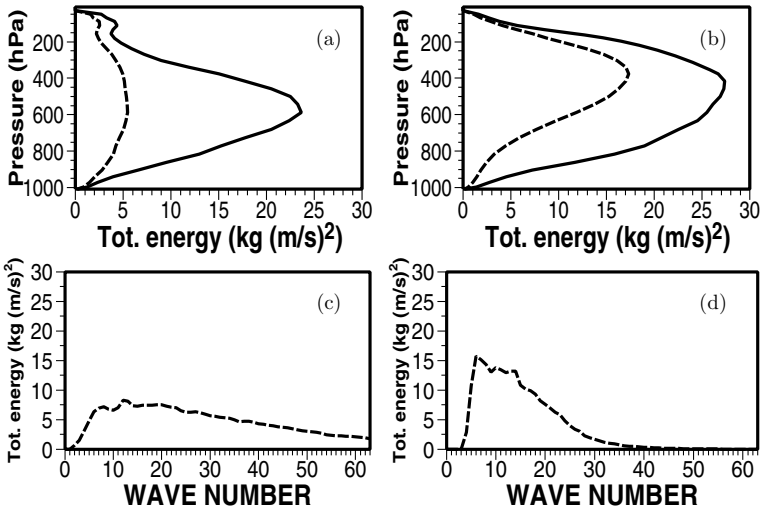

Fig. 4. (a and b) Vertical profiles of total energy and (c, d) the horizontal total energy spectrum in kg $m^2 s^{-2}$ for BGSENS, averaged over the 16-d OSSE period. The left/right-hand columns correspond to TE/**B**-matrix norm sensitivities. Dashed and solid lines in the top row correspond to kinetic and total energy, respectively.

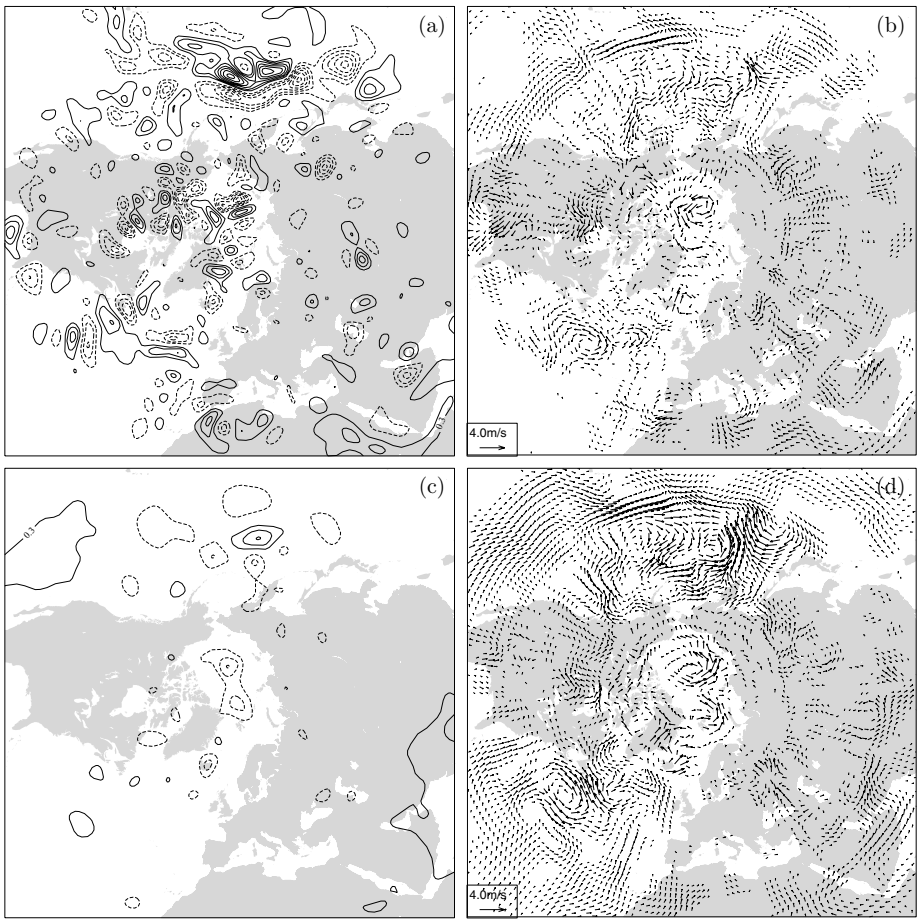

Fig. 5. Same as Fig. 2 but now for SOSE analysis adaptations, ANSOSE.

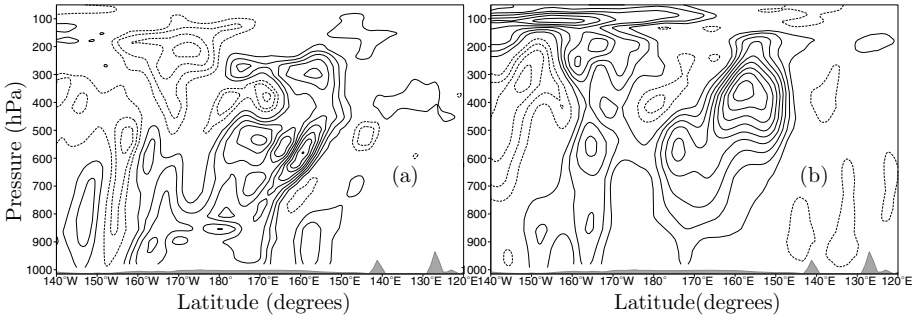

Fig. 6. Same as Fig. 3 but now for the analysis adaptation (ANSOSE).

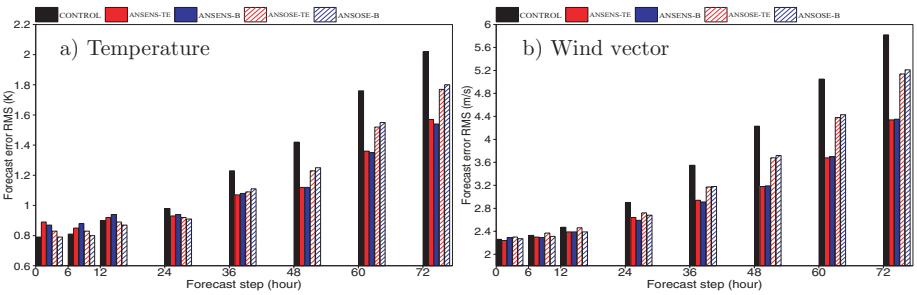

Fig. 7. 500 hPa RMS forecast error for (a) temperature and (b) wind averaged over the 16-d OSSE period. Forecast error is defined as the forecast minus the true atmospheric state from the nature run. The verification area is the Northern Hemisphere extra-tropics above 30° latitude. Forecasts are run from 12 UTC analyses obtained from (i) the uncorrected OSSE control analyses (black bars), and corrected control analyses according to (ii) TE norm perturbed analyses, ANSENS_TE, (red), (iii) **B**-matrix norm perturbed analyses, ANSENS_B, (blue), (iv) TE norm SOSE analysis, ANSOSE_TE, (red hatched) and (v) **B**-matrix norm SOSE analysis, ANSOSE_B, (blue hatched).

error is defined according to WMO standards by

$$\mathrm{RMSE}(x_f, x_t) = \sqrt{\frac{\sum_{i\in\Omega}[x_f(i) - x_t(i)]^2 \cos\phi_i}{\sum_{i\in\Omega}\cos\phi_i}}, \qquad (1)$$

with x_f the forecast value of the parameter under investigation, x_t the true atmospheric state (from the nature run) and ϕ_i denotes the latitude of gridpoint i. The summation is over all gridpoints inside the verification area Ω. In case of wind vector verification, the summation in the numerator contains two terms, that is, the eastward and northward wind components. From Fig. 7 it is clear that the operational TE and **B**-matrix norm sensitivity structures are equally well capable to reduce the 48-h forecast error (solid bars). This is an interesting result that confirms earlier findings that different analysis adaptations may give about equal forecast improvement. Also note that the improvement is not limited to the 48-h forecast, that is, the explicit objective of the sensitivity computation, but is retained for the subsequent day and even into the medium range and beyond (not shown). This is explained by the fact that a better forecast after 2 d delays the error growth on subsequent forecast days, Isaksen et al. (2005). However, from the forecast error in the range 0–48 h it is clear that ANSENS increase the forecast error in the first 24 h. In particular, at analysis time ANSENS draws the analyses away from the true atmospheric state on average. This is in agreement with Isaksen et al. (2005). The only exception is for TE wind sensitivities.

The hatched bars in Fig. 7 clearly demonstrate the trade-off of ANSOSE to constrain analysis errors on one hand (reduced forecast error at step 0) and to reduce the 48-h forecast error on the other hand. Yet, a forecast error reduction of about 12% (or about 10 h forecast range improvement) is still substantial.

Figure 8 also shows that the difference between ANSENS and ANSOSE is larger for temperature than for wind. This was expected since temperature sensitivities contribute most to the increased analysis error (black versus red/blue solid bars). Also, modifications are slightly larger for **B**-matrix norm sensitivities, yielding smaller analysis errors but at the expense of slightly larger forecast errors after day 2. Surprisingly, the analysis error of TE norm wind sensitivities is smaller for ANSENS than ANSOSE. In fact, ANSENS_TE wind adaptations, that are most pronounced over the data sparse oceans (not shown), decrease the analysis error, in particular over the data sparse oceans. Comparing Figs. 2b and 5b we note that the wind adaptations are larger in the latter. This may be explained by the imbalance of TE wind and temperature sensitivities that is compensated for in the analysis, giving larger (but artificial) adaptations.

It is interesting to note that the added variance by the adjoint sensitivity structures from ANSOSE_B does not degrade the analysis quality. From the numerical values in Fig. 8 it is

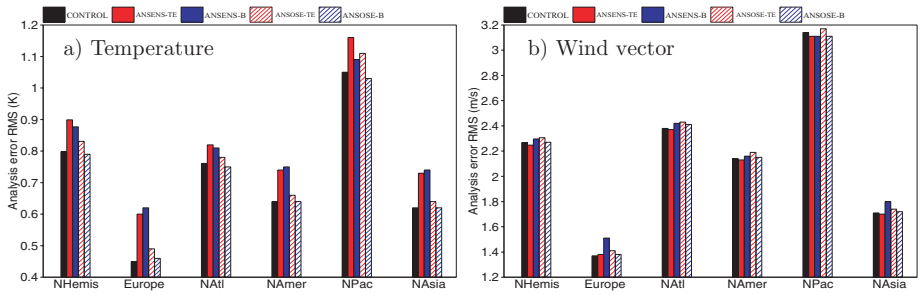

Fig. 8. Same as Fig. 7 but now for the 500 hPa analysis error (forecast step 0), and zoomed in on a number of global regions (N/S/W/E): NHemis (90/30/−180/180), Europe (75/35/−12/42), NAtl (75/20/−75/−5), NAmer (75/20/−130/−75), NPac (75/20/140/−120), Nasia (80/20/40/140). The numerical values for the NHemis bars are, respectively, 0.798/0.899/0.877/0.831/0.790 (K) for temperature and 2.267/2.247/2.296/2.306/2.270 (ms^{-1}) for wind.

found that that the analysis error has increased by 0.13% for wind while it has decreased by 1% for temperature. Strictly spoken the pseudo-truth from ANSOSE_B is closer to the truth than the control analysis on average although the sample is too small to demonstrate statistical significance. But, we stress that it is not a necessary requirement for the validity of the SOSE methodology to have the pseudo-truth closer to the truth than the control analysis. The pseudo-truth requirements have been clearly defined in the bullets R1–R3 in Section 2.

Figure 8a also shows that ANSENS_TE reduces the wind analysis error. The same is true in Fig. 8b for the temperature analysis error for ANSOSE_B. This is an interesting result showing that the analysis error has been reduced despite the increased variance that is brought into the system through the adaptation of the control analysis. This is further investigated. The analysis error is defined through $e = x_a^c - x_t$, with x_a^c the control analysis and x_t the true atmosphere, that is, the nature run for OSSE. The adapted analysis is defined through $x_a' = x_a^c + \epsilon_i$, with ϵ_i the analysis adaptation according to ϵ_1 = ANSENS_TE, ϵ_2 = ANSENS_B, ϵ_3 = ANSOSE_TE, and ϵ_4 = ANSOSE_B. The error variance of the adapted analysis is given by

$$\begin{aligned} \mathrm{var}(x_a' - x_t) &= \mathrm{var}(x_a^c - x_t + \epsilon_i) \\ &= \mathrm{E}(e + \epsilon_i)^2 - [\mathrm{E}(e + \epsilon_i)]^2 \\ &= \mathrm{E}(e^2) + \mathrm{E}(\epsilon_i^2) + 2\mathrm{E}(e\epsilon_i) - [\mathrm{E}(e + \epsilon_i)]^2 \\ &\approx \mathrm{var}(e) + \mathrm{var}(\epsilon_i) + 2\mathrm{cov}(e, \epsilon_i) \end{aligned} \quad (2)$$

where negligible biases have been assumed in the last step for simplicity and E and cov denote the expectation and covariance operators, respectively. The variances and covariance in eq. (2) have been computed for the 16-d OSSE period and summarized in Table 1. From the table some points are noteworthy. First, all correlation values, defined through $\rho(e, \epsilon_i) = \mathrm{cov}(e, \epsilon_i)/\sqrt{\mathrm{var}(e)\mathrm{var}(\epsilon_i)}$, are negative meaning that the analysis adaptations explain part of the analysis error. Yet, the correlation (covariance), that is, the last term on the right-hand side of eq. (2), is generally smaller than the added variance, that is, the second term on the right-hand side of eq. (2), and the overall result

Table 1. Variance of 500 hPa temperature (T) and wind (W) analysis adaptations, ϵ_i (see text for the definition), and their covariance and correlation with the control analysis error, e, for the Northern Hemisphere extra tropics above 30°N and computed for the 16-d OSSE period. The variance for the control analysis error, var (e), for temperature and wind equals 0.500 and 4.891, respectively. The numbers in italic format denote values smaller than the error in the control analysis, that is, where the analysis adaptation has reduced the analysis error

T/W	ϵ_1	ϵ_2	ϵ_3	ϵ_4
var (ϵ_i)	0.23/0.12	0.19/0.43	0.09/0.42	0.02/0.23
cov (e, ϵ_i)	−0.02/−0.10	−0.03/−0.16	−0.01/−0.13	−0.01/−0.11
$\rho(e, \epsilon_i)$	−0.07/−0.13	−0.10/−0.11	−0.05/−0.09	−0.13/−0.10
Eq. (2)	0.68/*4.81*	0.62/5.01	0.57/5.06	*0.49*/4.90

Table 2. List of acronyms. **B**-matrix refers to the background error covariance matrix

GOS	Global observing system
OSE	Observing system experiment
OSSE	Observing system simulation experiment
SOSE	Sensitivity observing system experiment
ANSENS	Default key analysis errors
ANSENS_TE	ANSENS based on total energy norm
ANSENS_B	ANSENS based on the **B**-matrix norm
BGSENS	Key background errors
BGSENS_TE	BGSENS based on total energy norm
BGSENS_B	BGSENS based on the **B**-matrix norm
ANCNTL	Control analysis
ANSOSE	Adaptation of the control analysis, This defines the SOSE analysis (pseudo-truth)
ANSOSE_TE	ANSOSE based on total energy norm
ANSOSE_B	ANSOSE based on the **B**-matrix norm

is an increase of the analysis error. There are two exceptions (in italic format in the table): the already mentioned ANSENS_TE wind and ANSOSE_B temperature. The negative correlation of the analysis error and the analysis adaptations may be explained by the mutual objective of the analysis and the sensitivity computation to determine a forecast initial state that improves the forecast. The small correlation values may be explained by the stochastic component of the analysis error that presumably dominates the dynamic component. Second, the correlation values are generally larger for **B**-matrix norm adaptations (third and fifth column) than for the total energy norm adaptations (second and fourth column). This is not surprising because **B**-matrix norm adaptations are found to be more realistic, since geostrophically balanced.

Here we note a limitation of the OSSE experiment that does not include (A)TOVS satellite radiance data, see Stoffelen et al. (2006). TOVS data define the temperature field over the oceans. Therefore we cannot conclude on a possible conflict between analysis adaptations and TOVS data. However, the amplitude of **B**-matrix norm temperature perturbations is generally small. In addition, from the left panel in Fig. 8 we note that **B**-matrix norm perturbations already draw the temperature to the true atmosphere over the oceans on average. Hence, we expect no conflict with TOVS data, if they would have been used. The same conclusion is not necessarily true for TE norm perturbations, because they have a larger amplitude for temperature and also show some negative impact over the oceans in the left-hand panel of Fig. 8.

Finally, ANSOSE_B are as close to the true atmospheric state as the operational analyses on average (black solid bar versus blue hatched bars). This is true, in particular over the data sparse oceans where ANSOSE are most pronounced, see Fig. 9. Also, adaptations are generally small over the continents which is a desired feature because analyses are generally good over data dense regions.

In conclusion, we have shown in this section that SOSE analyses using the **B**-matrix norm in the sensitivity computation are compatible with existing observations and maintain a substantial part of the forecast improvement capability, thus fulfilling the pseudo-truth requirements R1,R2.

2.2.2. Sensitivity realism. The final stage is to verify the realism of the spatial structures of the analysis adaptations produced

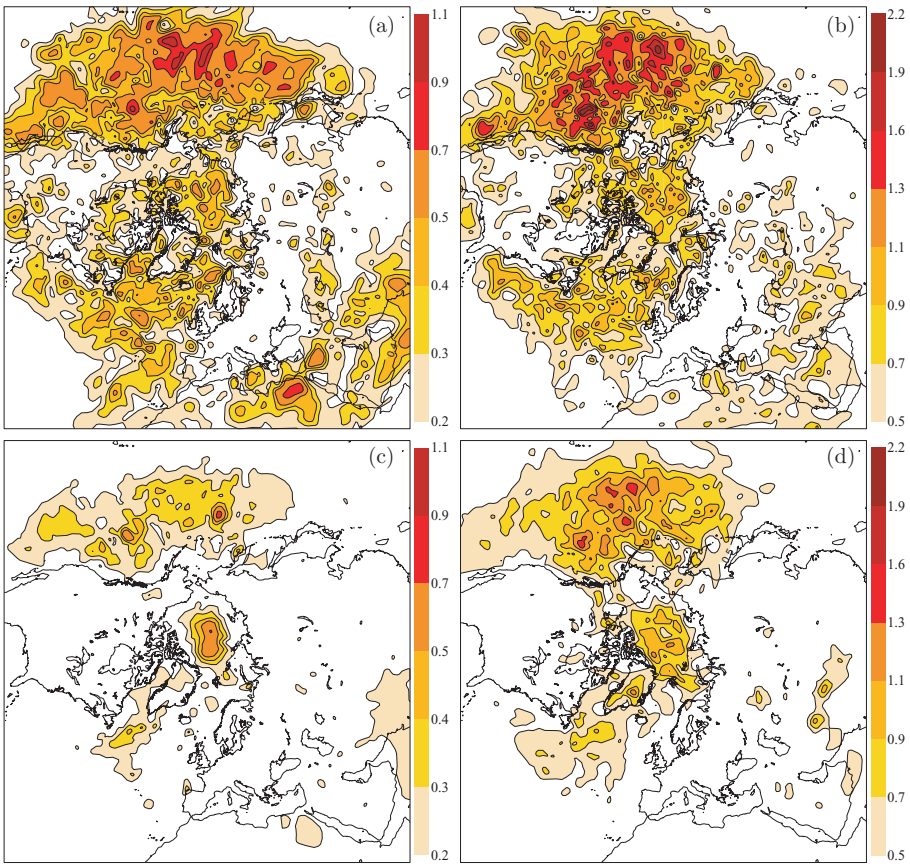

Fig. 9. 500 hPa RMS 9 UTC SOSE analysis adaptations, ANSOSE, averaged over the 16-d OSSE period. Sensitivity computations are based on (a, b) the TE norm and (c, d) the **B**-matrix norm. (a, c) Denote temperature (K) adaptations and (b, d) wind (ms^{-1}) adaptations.

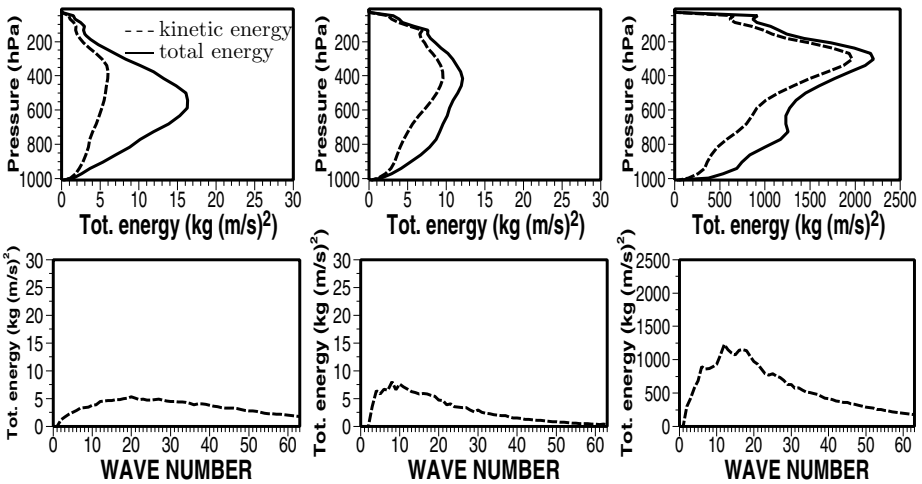

Fig. 10. Energy plots average over the 16-d OSSE period, similar as Fig. 4. The left/middle column corresponds to SOSE analysis adaptations from TE/**B**-matrix norm sensitivities. The right-hand column is for the true analysis error, that is, OSSE control analyses minus nature run.

in SOSE mode. This requires verification of the scales of the spatial structures of ANSOSE against those of real analysis errors. Such a verification is not feasible in operational practice since the true atmospheric state and thus the analysis error are unknown. In the OSSE framework the true atmospheric state is known through the nature run. Thus, it is easy to verify how well sensitivity structures compare with the true analysis error, since the latter is known explicitly as the difference between the analyses and nature run.

Comparing ANSENS in Figs. 4a and b with ANSOSE in Figs. 10a and b shows that the energy in the latter is about a factor of 30% less for the TE norm and about 50% for the **B**-matrix norm. This reduction is mainly caused by a suppression of sensitivity structures over the data dense continents. The amplitude of sensitivity structures is about a factor of 12 smaller than the true analysis error in Fig. 10c throughout the atmosphere. This is not surprising since sensitivities are constructed such that they represent the most rapidly growing analysis error structures, that is, the mean growth of true analysis errors will be much smaller.

The energy curves of the true analysis error are best resembled by ANSOSE_B with most of the energy in the kinetic part and a maximum in the higher troposphere above 400 hPa versus a mid-tropospheric maximum near 600 hPa for the TE norm. Also the smaller scales are better resembled in ANSOSE_B (Fig. 10e) than in BGSENS_B (Fig. 4d) which is the result of merging the background sensitivity adaptations with observations. As such, the spatial structures seem to resemble those of real analysis errors in Fig. 10f. Also, the shape of the energy spectra of ANSOSE_B matches quite well those of the analysis error. In conclusion, ANSOSE_B shares many aspects of the true analysis error:

(1) The vertical distribution and spatial scales of analysis errors are well represented;

(2) The geographical distribution of the analysis adaptations and true analysis error are concentrated over the data sparse oceans; and

(3) **B**-matrix norm sensitivities are meteorologically balanced by construction. However, since sensitivity structures represent only the fastest growing modes of the analysis adaptations, by construction the amplitude of sensitivities is much smaller than for analysis errors, maxima about 5 times smaller, hemispheric mean amplitudes are about 13 times smaller. A concern remains in the observability of the small structures by, for example, a DWL, but we show the successful forecast reduction in the remainder of this manuscript.

In conclusion, OSSE has proven a valuable framework to test various sensitivity concepts for the definition of a realistic pseudo true atmospheric state. A background sensitivity computation with the **B**-matrix norm constraint at initial time provides geostrophically balanced adaptations of the background. The corrected background is subsequently merged with observations from existing observing systems in the analysis to yield an atmospheric state fulfilling the pseudo-truth requirements (R1–R3). The SOSE analysis based on ANSOSE_B is therefore selected as a suitable candidate for the pseudo-truth.

3. SOSE observation usage

The pseudo-truth as defined in the previous section is used for the simulation of the new observing system under investigation. The resulting synthetic observations are used with existing observations in the analysis. In a well-tuned assimilation system, the information content of observations is well exploited, resulting in an analysis error covariance matrix that is smaller than the background error covariance matrix. This is true if a correct relative weight of the background state with respect to observations is given in the analysis, that is, for a properly chosen weight

matrix that includes the observation and background error statistics. The analysis equations for a SOSE experiment are described in the following section, culminating in a tuning procedure to give proper weight to the synthetic observations in SOSE.

3.1. SOSE—Mathematical framework

In numerical weather prediction (NWP) we look for the analysis state that is as close as possible to the true atmospheric state in the root-mean-square sense. Assuming linearity of the state equations and unbiased Gaussian distributed errors, the optimal least-squares estimate is found by the following equations, for example, Stoffelen et al. (2006).

$$x_a = x_b + \mathbf{K}[y - \mathbf{H}x_b] \tag{3}$$

$$y = \mathbf{H}x_t + r \tag{4}$$

with x_a the analysis, x_b the background and x_t the true atmospheric state, y the observations and r the observation error with covariance matrix $\mathbf{R}$. $\mathbf{H}$ is the linearized observation operator and $\mathbf{K} = \mathbf{B}\mathbf{H}^{\mathrm{T}}\ (\mathbf{H}\mathbf{B}\mathbf{H}^{\mathrm{T}} + \mathbf{R})^{-1}$ the (Kalman) gain matrix, including potential uncertainty in $\mathbf{H}$. $\mathbf{B} = \langle \epsilon_b \epsilon_b^{\mathrm{T}} \rangle$ is the background error covariance matrix, with ϵ_b the background error $\epsilon_b = x_b - x_t$ and $\langle\rangle$ denoting the expectation operator. The gain matrix $\mathbf{K}$ balances the weight of the background state estimate (through $\mathbf{B}$) and observations (through $\mathbf{R}$) in the analysis. Hence, low quality observations (large $\mathbf{R}$) will get less weight in the analysis. The Kalman gain is the optimal weight, in a statistical sense, applied to the innovation $(y - \mathbf{H}x_b)$ that minimizes the analysis error, when assuming unbiased Gaussian distributed errors Daley (1999), Lorenc (1986). The analysis error covariance matrix $\mathbf{A} = \langle \epsilon_a \epsilon_a^{\mathrm{T}} \rangle$, with $\epsilon_a = x_a - x_t$ may be written through

$$\mathbf{A} = [\mathbf{I} - \mathbf{K}\mathbf{H}]\mathbf{B}[\mathbf{I} - \mathbf{K}\mathbf{H}]^{\mathrm{T}} + \mathbf{K}\mathbf{R}\mathbf{K}^{\mathrm{T}} \tag{5}$$

and is smaller than $\mathbf{B}$ in a well-tuned data assimilation system.

Introducing subscripts and superscripts 'c' corresponding to conventional (existing) and 'd' for additional (synthetic) observations from the new instrument, eqs (3) and (4) turn into

$$x_a = x_b + \hat{\mathbf{K}}[\hat{y} - \hat{\mathbf{H}}x_b] \tag{6}$$

$$\hat{y} = \hat{\mathbf{H}}x_t + \hat{r} \tag{7}$$

with $\hat{y}$ the observation vector of the existing observations y_c augmented with the additional observations y_d and $\hat{r}$ the augmented observation error composed of r_c and r_d with corresponding observation error covariance matrix $\hat{\mathbf{R}}$ where we assume no correlation between the errors of the existing and additional observations, that is, $< r_c r_d^{\mathrm{T}} > = 0$. Next we define the augmented observation operator, $\hat{\mathbf{H}}$, and corresponding Kalman gain, $\hat{\mathbf{K}}$, through

$$\hat{\mathbf{H}} = \begin{bmatrix} \mathbf{H}_c \\ \mathbf{H}_d \end{bmatrix}$$

$$\hat{\mathbf{K}} = \mathbf{B}\hat{\mathbf{H}}^{\mathrm{T}} \left(\hat{\mathbf{H}}\mathbf{B}\hat{\mathbf{H}}^{\mathrm{T}} + \hat{\mathbf{R}}\right)^{-1}$$

$$= \mathbf{B}\left[\mathbf{H}_c^{\mathrm{T}} \mathbf{H}_d^{\mathrm{T}}\right] \begin{bmatrix} \mathbf{H}_c\mathbf{B}\mathbf{H}_c^{\mathrm{T}} + \mathbf{R}_c & \mathbf{H}_c\mathbf{B}\mathbf{H}_d^{\mathrm{T}} \\ \mathbf{H}_d\mathbf{B}\mathbf{H}_c^{\mathrm{T}} & \mathbf{H}_d\mathbf{B}\mathbf{H}_d^{\mathrm{T}} + \mathbf{R}_d \end{bmatrix}^{-1} \tag{8}$$

$$= \left[\hat{\mathbf{K}}_c \ \ \hat{\mathbf{K}}_d\right], \tag{9}$$

where $\hat{\mathbf{K}}$ has been split symbolically in two parts in the last step. Following the procedure to define the pseudo-truth as discussed in the previous section and definitions above, the analysis equation for the SOSE method is derived. First, the control analysis, using existing observation only, is given by

$$x_a^c = x_b + \mathbf{K}_c[y_c - \mathbf{H}_c x_b] \tag{10}$$

$$y_c = \mathbf{H}_c x_t + r_c \tag{11}$$

with $\mathbf{K}_c = \mathbf{B}\mathbf{H}_c^{\mathrm{T}}\ (\mathbf{H}_c\mathbf{B}\mathbf{H}_c^{\mathrm{T}} + \mathbf{R}_c)^{-1}$. The pseudo-truth x_t^p is defined as a perturbed control analysis

$$x_t^p = x_a^c + \delta \tag{12}$$

with δ the analysis adaptaton determined according to the procedure described in Fig. 1. Synthetic observations, y_d, of the new observing system are simulated using the pseudo-truth:

$$y_d = \mathbf{H}_d x_t^p + r_d. \tag{13}$$

From eq. (6) and using eq. (9) the resulting analysis from using both existing and new (synthetic) observations equals

$$x_a = x_b + \hat{\mathbf{K}}_c[y_c - \mathbf{H}_c x_b] + \hat{\mathbf{K}}_d[y_d - \mathbf{H}_d x_b]. \tag{14}$$

3.2. Application to spaceborne Doppler wind lidar

The procedure above was tested on a real case of a bad 2-d forecast of the ECMWF operational model over Europe verifying on 30 January 1999 12UTC. The corresponding SOSE wind analysis adaptation (δ) of the incorrect control analysis 2 d earlier is displayed in Fig. 11a. The pseudo-truth is the result of adding this adaptation to the control analysis, eq. (12). Next, 6 h of wind observations from the ESA Atmospheric Dynamics Mission polar orbiting satellite, named Aeolus, carrying a DWL were simulated using the pseudo-truth as input. Aeolus is scheduled for launch in late 2009 and will be operational for three years. The DWL instrument is a backscatter lidar measuring profiles of single horizontal line-of-sight (HLOS) wind components from the surface up to the lower stratosphere at about 30 km (Stoffelen et al., 2005). The simulation tool described in Marseille and Stoffelen (2003) has been used to simulate realistic observation

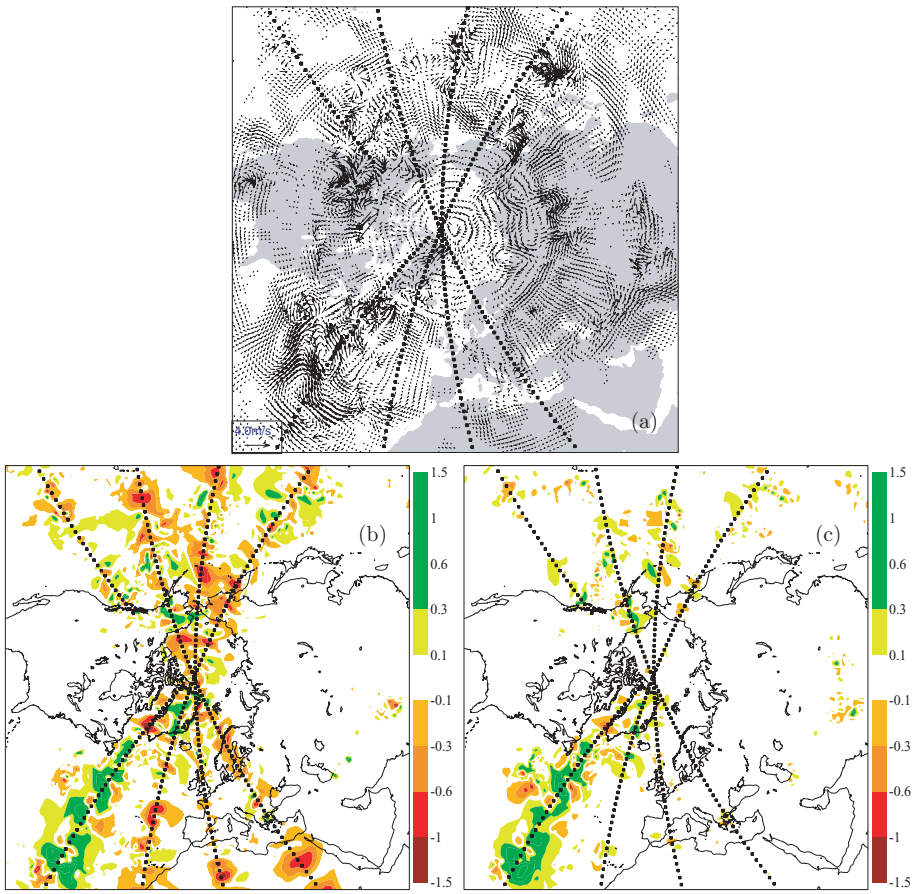

Fig. 11. (a) 500 hPa SOSE wind analysis adaptation from ANSOSE_B for 28 January 1999 12 UTC. Overlayed a 6-h coverage of ADM-Aeolus DWL observations. (b) DWL impact on wind analysis, that is, the difference of the analysis error of the control (no DWL) experiment and the analysis error of the DWL experiment. Analysis error is defined with respect to the pseudo-truth. Filled/dotted areas indicate positive/negative impact. The control experiment uses all existing observations, the DWL experiment synthetic DWL observations in addition. No weight correction was applied to the DWL observations. (c) same as (b) but now including a weight correction applied to the DWL observations in the analysis.

errors including instrument and representativeness error and taking into account cloud variability and cloud layering within the observed atmospheric volume. The synthetic DWL observations are subsequently used in the analysis together with all available observations from the existing observing systems. Negative analysis impact is found in Fig. 11b near DWL locations that correlate with areas of small analysis adaptations in Fig. 11a.

The negative DWL impact is explained by an incorrect respective weight of the synthetic DWL observations and the background in the analysis. This becomes clear when returning to eq. (8). Defining $\psi_c = \mathbf{H}_c\mathbf{B}\mathbf{H}_c^{\mathrm{T}} + \mathbf{R}_c$, $\psi_d = \mathbf{H}_d\mathbf{B}\mathbf{H}_d^{\mathrm{T}} + \mathbf{R}_d$ and $P = \mathbf{H}_c\mathbf{B}\mathbf{H}_d^{\mathrm{T}}$ and using the Sherman–Morrison–Woodbury matrix inversion lemma[1] it can be shown that the inverse of the matrix in eq. (8) equals

$$\begin{bmatrix} \psi_c & P \\ P^{\mathrm{T}} & \psi_d \end{bmatrix}^{-1} = \tag{15}$$

$$\begin{bmatrix} (\psi_c - P\psi_d^{-1}P^{\mathrm{T}})^{-1} & -\psi_c^{-1}P(\psi_d - P^{\mathrm{T}}\psi_c^{-1}P)^{-1} \\ -(\psi_d - P^{\mathrm{T}}\psi_c^{-1}P)^{-1}P^{\mathrm{T}}\psi_c^{-1} & (\psi_d - P^{\mathrm{T}}\psi_c^{-1}P)^{-1} \end{bmatrix}. \tag{16}$$

To keep the mathematics clear a simplification is introduced by assuming that $P = \mathbf{H}_d\mathbf{B}\mathbf{H}_c^{\mathrm{T}} = 0$. Physically this means that existing observations have no impact at locations of the additional observations and vice versa. This is correct if the distance between existing and synthetic observations is larger than the length-scale of the **B**-matrix structure functions. This used to be the case before the satellite era in data sparse areas over the oceans, that is, where the analysis adaptations δ are most

[1]Sherman–Morrison–Woodbury matrix inversion lemma $[\mathbf{A} + \mathbf{BCD}]^{-1} = \mathbf{A}^{-1} - \mathbf{A}^{-1}\mathbf{B}[\mathbf{DA}^{-1}\mathbf{B} + \mathbf{C}^{-1}]^{-1}\mathbf{DA}^{-1}$

pronounced. The validity is less clear in nowadays multivariate assimilation systems and the presence of satellite observations. Yet, we apply the simplification for illustration purposes only and not as a general rule in nowadays data assimilation. Setting $P = 0$ simplifies eq. (16) to

$$\begin{bmatrix} \psi_c^{-1} & 0 \\ 0 & \psi_d^{-1} \end{bmatrix} = \begin{bmatrix} (\mathbf{H}_c\mathbf{B}\mathbf{H}_c^{\mathrm{T}} + \mathbf{R}_c)^{-1} & 0 \\ 0 & (\mathbf{H}_d\mathbf{B}\mathbf{H}_d^{\mathrm{T}} + \mathbf{R}_d)^{-1} \end{bmatrix}. \tag{17}$$

Substituting in eq. (8) yields $\hat{\mathbf{K}}_c = \mathbf{K}_c$ and similarly $\hat{\mathbf{K}}_d = \mathbf{K}_d = \mathbf{B}\mathbf{H}_d^T(\mathbf{H}_d\mathbf{B}\mathbf{H}_d^T + \mathbf{R}_d)^{-1}$. In addition, from eq. (10), $\mathbf{H}_d x_a^c = \mathbf{H}_d x_b$ since $\mathbf{H}_d\mathbf{K}_c = \mathbf{H}_d\mathbf{B}\mathbf{H}_c^{\mathrm{T}}\,(\mathbf{H}_c\mathbf{B}\mathbf{H}_c^{\mathrm{T}} + \mathbf{R}_c)^{-1} = 0$. With this approximation, eq. (14) becomes

$$x_a = x_b + \mathbf{K}_c[y_c - \mathbf{H}_c x_b] + \mathbf{K}_d[y_d - \mathbf{H}_d x_b] \tag{18}$$

$$= x_a^c + \mathbf{K}_d\big[y_d - \mathbf{H}_d x_a^c\big]. \tag{19}$$

Equations (13) and (19) show large similarity to eqs (3) and (4), with the background replaced by the control analysis, resulting from using existing observations, and using synthetic observations in the innovation only. The analysis error covariance matrix with respect to the pseudo-truth yields

$$\Big\langle \big(x_a - x_t^p\big)\big(x_a - x_t^p\big)^{\mathrm{T}} \Big\rangle = [\mathbf{I} - \mathbf{K}_d\mathbf{H}_d]\langle\delta\delta^{\mathrm{T}}\rangle[\mathbf{I} - \mathbf{K}_d\mathbf{H}_d]^{\mathrm{T}} + \mathbf{K}_d\mathbf{R}_d\mathbf{K}_d^{\mathrm{T}} \tag{20}$$

Note the similarity between eqs (20) and (5), where $\mathbf{B}$ has been replaced by $\langle\delta\delta^{\mathrm{T}}\rangle$. For regions where perturbations are small $\langle\delta\delta^{\mathrm{T}}\rangle \approx 0$ and consequently $\langle(x_a - x_t^p)(x_a - x_t^p)^{\mathrm{T}}\rangle \approx \mathbf{K}_d\mathbf{R}_d\mathbf{K}_d^{\mathrm{T}}$ according to eq. (20). In other words, the analysis error with respect to the pseudo-truth over these regions is dominated by the observation error of the new instrument that will generally be larger than the perturbations, thus giving negative impact of the new observing system if not well tuned.

3.3. Observation weight correction

As a consequence of the analysis above, for an optimal use of the new observing system in SOSE, the weight of synthetic observations in the assimilation needs to be tuned over regions of small analysis adaptations to prevent negative impacts. Without tuning, analysis errors will increase in regions where the perturbations are small, mainly because of the applied stochastic errors in the observations. This is caused by an incorrect respective weight of the synthetic DWL observations and the background. This can be explained by noting that in a regular analysis procedure the error of the background field is reduced by observational information through a Kalman gain that optimally weights the background and observation error. In a SOSE the uncertainty is determined by the perturbation amplitude rather than the background error. In regions of negligible analysis adaptation, $\delta \approx 0$, the conventional observations draw the analysis close to the pseudo-truth that is close to the control analysis according to eq. (12). Then the synthetic observations mainly carry the control analysis and a synthetic observation random error, that is, they add no new information on the atmospheric state and their weight in the analysis should be reduced. This becomes clear when considering the analysis equation, eq. (3), in one dimension

$$x_a = x_b + k[y - hx_b] \tag{21}$$

$$= (1 - kh)x_b + ky \tag{22}$$

$$= \frac{\sigma_o^2}{\sigma_b^2 + \sigma_o^2}x_b + \frac{\sigma_b^2}{\sigma_b^2 + \sigma_o^2}y \tag{23}$$

with σ_b and σ_o the background and observation error standard deviation, respectively, and by setting the observation operator h equal to identity. In a SOSE, the background x_b in eq. (23) is replaced by x_a^c, that is, the analysis using all conventional observations, see eq. (19). Then, the weight of the observations, $\sigma_b^2/(\sigma_b^2 + \sigma_o^2)$, is generally too large at locations where the perturbation δ is small, because x_a^c is already a very good estimate of the pseudo true atmosphere, see eq. (12). To correct for this we force the analysis to use a different weight than the usual value based on the observation error standard deviation, as follows

$$\sigma_o^* = \sigma_o\frac{\sigma_b}{|\delta|}. \tag{24}$$

The analysis equations eqs (21)–(23) are applied again but now using the corrected weight for the observation. The corrected observation weight factor, k^*, then equals $k^* = \sigma_b^2/(\sigma_b^2 + \sigma_o^{*2}) = 1/(1 + \sigma_o^{*2}/\sigma_b^2) = 1/(1 + \sigma_o^2/\delta^2)$. Similarly the weight factor of the background equals $(1 - hk^*) = \sigma_o^{*2}/(\sigma_b^2 + \sigma_o^{*2}) = \sigma_o^2/(\sigma_o^2 + \delta^2) = 1/(1 + \delta^2/\sigma_o^2)$. Hence for $\delta \approx 0$, $k^* \approx 0$ thus giving no weight to the additional (synthetic DWL) observations and thus leaving the control analysis unchanged as desired.

In summary, the observation error standard deviation σ_o includes instrument and representativeness errors and is used for the simulation of the synthetic observation while σ_o^* is the corrected value that is used to determine the weight of that observation in the analysis. The result of this correction is that the weight given to the synthetic observations is proportional to $(\delta/\sigma_o)^2$ rather than the usual $(\sigma_b/\sigma_o)^2$. Physically this is explained by noting that the objective of observations in the analysis is to reduce the variance of the background error while in SOSE the objective of the additional synthetic observations is to reduce the added variance brought into the system through the adaptation of the control analysis, that is, the part of the analysis error that is not observed by the existing network.

Although background errors vary with geographical location and since its true value is unknown, we use a constant scalar value for the background error in the weight correction computation for simplicity. A suitable value of 1.4 ms^{-1} for σ_b in eq. (24) was found empirically for the case discussed in Fig. 11 by checking the wind analysis impact of Aeolus for a range of values for σ_b. This value corresponds quite well with typical

mid-tropospheric wind component background errors in nowadays NWP models. To prevent unrealistic large weights for DWL at locations of relatively large adaptations, and thus introducing noise in the resulting analysed atmospheric state, the value for δ in eq. (24) is maximized by an empirically selected value of $4\sigma_b$. However, this constraint is hardly met since wind adaptations in active sensitive regions do generally not exceed 2 ms^{-1}, see for example, Figs. 5d and 11a. As a consequence, the weight of DWL observations in SOSE will generally be close to the weight that would be given in operational NWP to DWL data over data sparse areas.

Returning to the full dimensional system and using the corrected weights in the gain matrix yields $\psi_d = \mathbf{H}_d\mathbf{B}\mathbf{H}_d^{\mathrm{T}} + \mathbf{R}_d^*$ in eq. (16). The diagonal elements of $\mathbf{R}_d^*$ are given by $\mathbf{R}_d^*(i, i) = \mathbf{R}_d(i, i)\sigma_b^2/\delta(i)^2$. For σ_b we used the scalar value of 1.4 ms^{-1} as determined above and $\delta(i)$ is the analysis adaptation at the location of the ith synthetic observation. For the unlikely event that δ approaches zero at each location, all diagonal elements of ψ_d go to infinity and only the top left matrix in eq. (16) will not vanish to zero. The resulting analysis then equals the control analysis, eq. (10), as desired because the additional (synthetic) observations add no information to the system. Otherwise, in case that δ is close to zero for a limited number of observations, the upper left matrix is completely filled while the other three are block matrices with those rows and columns filled with zeroes corresponding to observation locations where $\delta = 0$. These observations have zero weight in the analysis as desired.

Figure 11c shows the impact of Aeolus but now using corrected weights for the synthetic DWL observations in the analysis. Clearly, the areas of negative impact have been reduced substantially, while areas of positive impact are maintained to a large extent with some minor reduced improvement locally. The mean Northern Hemisphere impact has turned from negative (-0.02 ms^{-1}) to positive (0.01 ms^{-1}). In particular, the impact over the North Atlantic has increased from 0.02 to 0.05 ms^{-1}. As a result, 6 h of DWL data has reduced the mean 500 hPa 2-d forecast error of the geopotential height over Europe (not shown) from 42.81 m (operational 2-d forecast error) to 42.55 m, without observation weight correction, and to even 42.11 m, including observation weight correction. We point out that a complete recovery of the analysis perturbation would reduce the forecast error to 38.39 m which corresponds to the best achievable forecast for this case. Therefore, observation weight tuning in the analysis has reduced the forecast error substantially from 6 to 16%.

3.4. SOSE—calibration

Calibration is usually carried out to investigate the impact of simulated observations to verify the experimental setup and the realism of the results. Calibration is an important aspect of SOSE when absolute impact results are required. The first aspect is to verify the analysis impact of the different observing systems. We verify the use of observations in the experiment with operations through the distributions of observation minus background (o-b) and observation minus analysis (o-a) statistics and the observation rejection rate. For the case discussed in the previous section no substantial discrepancies were found in the data usage statistics of the CONTROL (no DWL) and DWL experiment for the existing observations. Although applied to a single case, this result is a strong indication of a valid setup of the SOSE experiment: the new observing system (DWL) is capable to resolve (part of) the additional variance brought into the system, through the analysis adaptation that defines the pseudo-truth, but without disturbing the existing observations. This is fully in line with the SOSE pseudo-truth requirements defined in Section 2.

4. Summary, conclusions and discussion

One of the ultimate goals in operational meteorology is to reduce the occurrence of large forecast failures, in particular, those with large socio-economic impact. Forecast failures on the short term are mainly caused by deficiencies of the current GOS, being non-uniform, lacking observations over the Southern Hemisphere, Tropics and Northern Hemisphere oceans. Atmospheric structures in these regions that tend to grow rapidly in time are not well observed potentially causing large forecast failures already on the short term (up to 2 d). International programs like THORPEX show a growing interest to define observation strategies that increase the accuracy of high-impact weather forecasts.

In this paper, a new method to assess the added value of new observations to the GOS is presented, named SOSE. SOSE is a useful tool to test optional extensions to the GOS. It may address fundamental questions related to observation strategies such as the relative merit of observation targeting strategies in pre-determined meteorologically sensitive areas versus a continuous and spatially uniform sampling of the atmosphere from space. In addition, SOSE can be applied to real extreme events with forecast failures in the past to test the impact of various observation strategies. Results may be used for the definition of observation requirements culminating in instrument design concepts for prospective (spaceborne) observing systems to extend the GOS. A companion paper applies SOSE to compare various prospective DWL scenarios for the definition of an operational DWL mission in the post-ADM era, beyond 2012. However, SOSE is in principle applicable to any (future) observing system.

The fact that SOSE needs only the simulation of the new observations makes it an effective tool as compared to, for example, a full-blown OSSE that requires the simulation of all existing observing systems in addition, including the increasing number of satellite systems.

In a SOSE, adjoint sensitivity structures are used to define a so-called 'pseudo-true' atmospheric state for the simulation of the prospective observing system(s). A simplified approach to force compatibility of the pseudo-truth with existing observations

is used for practical reasons. The constraint could also be applied more directly by adopting an observation term in eq. (25) or alternatively by iterating the sensitivity computation. Within an OSSE framework it has been verified that the pseudo-truth is (i) a better forecast initial state, (ii) compatible with existing observations including from satellite systems and (iii) the spatial scales of the analysis adaptation, to generate the pseudo-truth, are realistic, that is, resembling those of real analysis errors. The analysis adaptations represent atmospheric structures not resolved by the existing GOS. It is shown that the adjoint sensitivity structures in the OSSE are weakly correlated with the analysis error, presumably because part of the dynamic analysis error is resolved. This is encouraging, since one would not expect adjoint predictability of small-scale deterministic structures over 2 d. However, as expected, the analysis error appears dominated by stochastic error variance and total error variance effects are small.

The pseudo-truth is subsequently used for the simulation of additional observations, for example, from a prospective satellite observing system or based on targeting strategies. The synthetic observations are used together with real observations in the analysis and when the new observations are capable to (partly) resolve the analysis adaptations they will contribute to improve the forecast. The construction of the analysis adaptations is such that synthetic observations do not conflict with existing observations; over data dense areas where the control analysis is already good the amplitude of the analysis adaptation is generally small. Consequently, not to increase the stochastic analysis error after assimilation of the noisy synthetic observations, their weight is reduced in the analysis over regions where the analysis adaptations are small and no observation impact is expected.

An application of SOSE demonstrated the capability of wind observations from a future space borne DWL to improve the analysis and subsequent forecast. Observation and analysis impact statistics of existing observations have been compared with those from the control run and no discrepancies were found, a strong indication of a valid experimental setup of SOSE: the additional variance brought into the system through the analysis adaptations has been recovered (partly) by DWL without disturbing the existing observations.

In SOSE only part of the 2-d forecast error is exploited. The adjoint computation uses the NWP model and its adjoint as a strong constraint. As such, that part of the forecast error due to model errors remains present. Moreover, due to the strong constraint, errors in the adjoint computation may further reduce forecast error reduction capability. A third issue may be in the fact that model errors are compensated for by adaptations to the initial state. However, there is no indication that the analysis adaptation mainly corrects for model deficiencies rather than for realistic flow-dependent error structures. Singular vector computations indicate that locations of error growth show a large similarity for different models, for example, Gelaro et al. (2000). This indicates a flow dependency rather than a model dependency. NWP models have improved substantially over the last decades and it is expected that their error characteristics are similar and resemble those of real analysis errors as elaborated in Section 2.2.2 These are the structures that new observations should be able to resolve to have a positive impact in operational NWP. It is therefore expected that observation impact will not dramatically differ when SOSE is applied to another system and we expect that conclusions on observation impact will be similar for different NWP models.

On the other hand, there is yet no evidence how beneficial synthetic SOSE observations would be when used in a foreign data assimilation system and forecast model. It may be that the generation, location and evolution of analysis adaptations is model dependent. The beneficial impact of synthetic SOSE observations generated and used in one assimilation system would then perhaps be less when impact is tested in a different data assimilation system.

Applying a weak constraint approach in a SOSE probably is likely to result in a more significant compensation of model error and at the same time a further reduction of the 2-d forecast error. This method has been implemented at ECMWF (Barkmeijer et al., 2003).

Although initially developed to test potential additions to the GOS to reduce its deficiencies SOSE could be used to test the substitution of existing systems with new technology, for example, by generating a pseudo-truth without using the existing system followed by two experiments, one with simulated observations from the existing system and the other based on the new technology. We did not test this option, because alternative replacement experiments (OSRE) already exist, for example, Cress and Wergen (2001). Such experiment is recommended for absolute SOSE calibration though.

The described SOSE implementation is a single cycle experiment, meaning that synthetic observations are added in only one assimilation window. As such the observation impact is not fully representative for the expected impact of the observing system in operational NWP, since data assimilation systems are capable to propagate information from observations forward in time to next cycles in a constructive manner and as such increase the impact of the observations under investigation. However, single-cycle SOSE is useful to compare the *relative* impact of various observing system sampling scenarios.

For a more absolute impact assessment of prospective observing systems in real extreme events, the SOSE method needs to be applied in so-called cycling mode to take advantage of observations by the new observing system in the time prior to the event. An example is discussed in a separate paper, Marseille et al. (2007).

The discussion in this paper has been limited to the Northern Hemisphere extra-tropics but is in principle also applicable to the Southern Hemisphere and tropics. For the latter, implementation of a wet sensitivity computation (including humidity in the norm definition) for the definition of the pseudo-truth seems logical to

account for moist processes that are more dominant in the tropics than extra-tropics.

5. Acknowledgments

This paper is the result of the project Prediction Improvement of Extreme Weather (PIEW) funded by the European Space Agency (ESA). The authors thank ESA and members of the Aeolus Mission Advisory Group for stimulating discussions. Special thanks go to the ECMWF staff, in particular Erik Andersson, Hans Hersbach and Sami Saarinen for technical support to run the OSSE experiment with a recent model cycle.

6. Appendix: computation of adjoint sensitivity structures

Sensitivity structures are the result of minimizing a cost function J that is defined as a norm of the forecast error (forecast minus verifying atmospheric state). Following the notation of Isaksen et al. (2005)

$$J_t(\delta\mathbf{x}_0) = \frac{1}{2}\|\mathbf{P}(\mathcal{M}_t(\mathbf{x}_0+\delta\mathbf{x}_0)-\mathbf{x}_t)\|_A^2 \tag{A.1}$$

with matrix $\mathbf{A}$ defining the norm at final (verification) time; $\|\mathbf{x}\|_A^2 = \mathbf{x}^{\mathrm{T}}\mathbf{A}\mathbf{x}$), x_0 the forecast initial state at time t_0 and x_t the verifying atmospheric state 48 h later at $t = t_0 + 48$, $\delta\mathbf{x}_0$ is the forecast initial state correction (or perturbation) and $\mathcal{M}_t$ is the non-linear forecast model integrating the perturbed initial state $\mathbf{x}_0 + \delta\mathbf{x}_0$ forward in time. $\mathbf{P}$ represents a projection on the targeted area, in our experiments the Northern Hemisphere extra-tropics above 30°N. In operational mode, x_0 is the analysis while in the SOSE method, x_0 is the background. A suitable metric for the final time norm is the dry total energy (TE) norm that is defined as an integral on the sphere according to Rabier et al. (1993); Palmer et al. (1998)

$$\|\mathbf{x}\|_A^2 = \frac{1}{2}\int_\eta\int_\Sigma\left[u^2+v^2+\frac{C_p}{T_r}T^2\right]\mathrm{d}\Sigma\left(\frac{\partial p}{\partial\eta}\right)\mathrm{d}\eta + \frac{1}{2}\int_\Sigma R_a T_r(\ln p_s)^2\,\mathrm{d}\Sigma \tag{A.2}$$

with $\mathbf{x}$ defining the atmospheric state with components u, v, p_s and T, that is, the zonal and meridonal wind components, surface pressure and temperature, respectively, p is pressure, Σ denotes the horizontal integration domain on the sphere, η is the vertical coordinate, T_r is a reference temperature set at 300° Kelvin and R_a and C_p are thermodynamic constants for the gas constant for dry air and dry air specific heat, respectively; $R_a = 287\ \mathrm{JK}^{-1}\ \mathrm{kg}^{-1}$, $C_p = 1004\ \mathrm{JK}^{-1}\ \mathrm{kg}^{-1}$.

Isaksen et al. (2005) showed that under the assumption of a perfect forecast model the initial time gradient with respect to the inner product defined by matrix $\mathbf{A}$ equals

$$\nabla_A J_0 = \mathbf{M}^*\nabla_A J_t \tag{A.3}$$

with the final time gradient $\nabla_A J_t = -\mathbf{P}(\mathcal{M}_t(\mathbf{x}_0+\delta\mathbf{x}_0)-\mathbf{x}_t)$ from eq. (A.1) and $\mathbf{M}^*$ the adjoint of the tangent linear model $\mathbf{M}$.

Equations (A.1) and (A.2) relate forecast initial state to forecast errors on the targeted area. As a first order approximation, a change $\delta\mathbf{x}_0$ in the initial conditions $\mathbf{x}_0$ through $\delta\mathbf{x}_0 \propto -\nabla_A J_0$ results in a reduction of the forecast error by $\delta J_t = \nabla_A J_0^{\mathrm{T}}\,\delta\mathbf{x}_0 \propto -\|\nabla_A J_0\|^2$. This means that in regions where the gradient $\nabla_A J_0$ is large, a change in the initial conditions yields a large reduction of the forecast error. In other words, the pattern of the gradient of J_t at initial time shows the sensitivity of the forecast error to the initial conditions. As explained in Rabier et al. (1996) the gradient corresponds to rapidly growing components of the analysis error.

To constrain the spatial structures of the perturbation $\delta\mathbf{x}_0$ at initial time an additional constraint is imposed defined by a norm $\|\mathbf{x}\|_C$ for some matrix $\mathbf{C}$, see Klinker et al. (1998)

$$\|\delta\mathbf{x}_0\|_C = \epsilon \tag{A.4}$$

for some small constant value ϵ. Isaksen et al. (2005) show that the gradient of the cost function with respect to an initial time inner product, defined by $\mathbf{C}$, is given by

$$\nabla_C J_0 = \mathbf{C}^{-1}\mathbf{A}\nabla_A J_0 \tag{A.5}$$

In this paper two initial time norms are considered:

(1) The TE-norm, eq. (A.2), that is, $\mathbf{C} = \mathbf{A}$. Palmer et al. (1998) concluded that of three simple norms in the form of diagonal operators the TE norm gave sensitivity structures bearing the largest resemblance with the spatial scales of analysis errors.

(2) The background error covariance matrix norm, in the remainder denoted $\mathbf{B}$-norm, that is, $\mathbf{C} = \mathbf{B}^{-1}$, that explicitly imposes a correct balance between temperature and wind perturbations, Barkmeijer et al. (1999).

Minimization of the cost function is done iteratively. It was found empirically by Klinker et al. (1998) that 3–6 iterations provide most realistic spatial structures of the resulting key analysis errors. Computation of the cost function gradient at initial time requires integration of the adjoint model as explained in, for example, Le Dimet et al. (1986); Rabier et al. (1993, 1996). The adjoint integrations in this paper are performed with the linearized model at T63L60 resolution (about 300-km horizontal resolution and 60 vertical levels) in the vicinity of the trajectory as derived by a non-linear forward integration. The linearity assumption limits sensitivity computations to forecast ranges up to 48 h for which the growth of small perturbations is well approximated.

References

Barkmeijer, J., Buizza, R. and Palmer, T. N. 1999. 3D-Var Hessian singular vectors and their potential use in the ECMWF Ensemble Prediction System. *Q. J. R. Meteorol. Soc.* **125**, 2333–2351.

Barkmeijer, J., Iversen, T. and Palmer, T. N. 2003. Forcing singular vectors and other sensitive model structures. *Q. J. R. Meteorol. Soc.* **129**, 2401–2423.

Bergot, T., Hello, G., Joly, A. and Malardel, S. 1999. Adaptive observations: a feasibility study. *Mon. Wea. Rev.* **127**, 743–765.

Caron, J. F., Yau, M. K., Laroche, S. and Zwack, P. 2007. The characteristics of key analysis errors. Part I: dynamical balance and comparison with observations. *Mon. Wea. Rev.* **135**, 249–266.

Cress, A. and Wergen, W. 2001. Impact of profile observations on the German Weather Service's NWP system. *Meteor. Zeitschrift* **10**, 91–101.

Daley, R. 1999. Atmospheric Data Analysis. *Cambridge Atmospheric and Space Science Series*, Cambridge University Press, Cambridge, UK. ISBN 0-521-45825-0, 457 p.

Fisher, M., 2003. Background error covariance modelling. In: *Proceedings of ECMWF Seminar "Recent developments in data assimilation for atmosphere and ocean, 8–12 September 2003", Reading, UK*, 45–64.

Gelaro, R., Reynolds, C. A., Langland, R. H. and Rohaly, G. D. 2000. A Predictability Study Using Geostationary Satellite Wind Observations during NORPEX. *Mon. Weather Rev.* **128**, 3789–3807.

Hello, G., Lalaurette, F. and Thépaut, J. N. 2000. Estimation of key analysis errors using the adjoint technique. *Q. J. R. Meteorol. Soc.* **126**, 621–647.

Isaksen, L., Fisher, M., Andersson, E. and Barkmeijer, J. 2005. The structure and realism of sensitivity perturbations and their interpretation as "Key Analysis Errors". *Q. J. R. Meteorol. Soc.* **131**, 3053–3078.

Kelly, G. 2004. OSEs of all main data types in the ECMWF operational system. In: *Proceedings of the Third WMO Workshop on the Impact of Various Observing Systems on NWP, Alpbach, Austria*, 63–94.

Klinker, E., Rabier, F. and Gelaro, R. 1998. Estimation of key analysis errors using the adjoint technique. *Q. J. R. Meteorol. Soc.* **124**, 1909–1933.

Koch, R., Ehrendorfer, M. and Weissmann, M. 2006. Key analysis errors and airborne LIDAR measurements of wind. http://www.pa.op.dlr.de/na-trec/KochEtAl2006_poster.pdf

Le Dimet, F. and Talagrand, O. 1986. Variational algorithms for analysis and assimilation of meteorological observations: theoretical aspects. *Tellus* **38A**, 97–110.

Lorenc, A. 1986. Analysis methods for numerical weather prediction. *Q. J. R. Meteorol. Soc.* **112**, 1177–1194.

Marseille, G. J. and Stoffelen, A. 2003. Simulation of wind profiles from a space-borne Doppler wind lidar. *Q. J. R. Meteorol. Soc.* **129**, 3079–3098.

Marseille, G. J., Stoffelen, A. and Barkmeijer, J. 2007. A cycled sensitivity observing system experiment on simulated Doppler wind lidar data during the 1999 Christmas storm "Martin". *Tellus* **60**, doi: 10.1111/j.1600-0870.2007.00290.x.

Masutani, M., Lord, S. J., Woollen, J. S., Yang, W., Sun, H., and co-authors. 2004. Global OSSE at NCEP. In: *Proceedings of the Eighth Symposium on Integrated Observing and Assimilation Systems for Atmosphere, Oceans, and Land Surface* AMS, Seattle, USA

Palmer, T. N., Gelaro, R., Barkmeijer, J. and Buizza, R. 1998. Singular vectors, metrics, and adaptive observations. *J. Atmos. Sci.* **55**, 633–653.

Rabier, F., Courtier, P., Herveou, M., Strauss, B. and Persson, A. 1993. Sensitivity of forecast error to initial conditions using the adjoint model. *ECMWF Technical Memorandum* **197**.

Rabier, F., Klinker, E., Courtier, P. and Hollingsworth, A. 1996. Sensitivity of forecast errors to initial conditions. *Q. J. R. Meteorol. Soc.* **122**, 121–150.

Rabier, F., Järvinen, H., Klinker, E., Mahfouf, J.-F. and Simmons, A. 2000. The ECMWF operational implementation of four-dimensional variational assimilation. I: experimental results with simplified physics. *Q. J. R. Meteorol. Soc.* **126**, 1143–1170.

Shapiro, M. and Thorpe, A. 2004. THORPEX International Science Plan, vs. 3. *WMO/TD-No. 1246, WWRP/THORPEX No. 2*.

Stoffelen, A., Pailleux, J., Källén, E., Vaughan, J. M., Isaksen, L., and co-authors. 2005. The Atmospheric dynamics mission for global wind measurement. *Bull. Am. Meteorol. Soc.* **86**, 73–87.

Stoffelen, A., Marseille, G. J., Bouttier, F., Vasiljevic, D., de Haan, S. and Cardinali, C. 2006. ADM-Aeolus Doppler wind lidar Observing System Simulation Experiment. *Q. J. R. Meteorol. Soc.* **132**, 1927–1947.

Tan, D. G. H., Andersson, E., Fisher, M. and Isaksen, L. 2007. Observing system impact assessment using a data assimilation ensemble technique: application to the ADM-Aeolus wind profiling mission. *Q. J. R. Meteorol. Soc.* **133**, 381–390.

Trémolet, Y. 2006. Accounting for an imperfect model in 4D-Var. *Q. J. R. Meteorol. Soc.* **132**, 2483–2504.

WMO, 2004. Current Statement of Guidance Regarding How Well Satellite Capabilities Meet WMO User Requirements in Ten Application Areas. *WMO satellite reports*.